PAPER

Check for updates

Synthesis of a novel magnetic biochar composite enhanced with polyaniline for high-performance adsorption of heavy metals: focus on Hg(II) and Cu(II)†

Rzgar Kareem,[a] Abbas Afkhami [ID] *[a] and Kosar Hikmat Hama Aziz [ID] *[bc]

This study explores the potential of using magnetic biochar derived from sesame seed cake (PMBS) and enhanced with polyaniline (PANI) for the removal of heavy metals from aqueous solutions. The synthesized PMBS was comprehensively characterized and evaluated as an effective adsorbent for Hg^{2+} and Cu^{2+} removal. This study assessed various physicochemical properties, including surface morphology, porosity, specific surface area, chemical composition, valence states, and magnetic characteristics, of the composite to determine its efficacy in heavy metal removal from wastewater. The adsorption performance of the magnetic biochar was significantly enhanced *via* PANI doping. Furthermore, the easy magnetic recovery of PMBS from aqueous solutions after adsorption was successfully demonstrated using an external magnetic field. The adsorption kinetics of heavy metal ions on PMBS followed a pseudo-second-order model, while Langmuir isotherm analysis confirmed monolayer adsorption behavior. The maximum adsorption capacities for Hg^{2+} and Cu^{2+} were determined to be 141.89 and 124.78 mg g^{-1}, respectively. The electrochemical measurements of square wave anodic stripping voltammetry (SWASV) were employed to determine residual metal ion concentrations after adsorption. Calibration curves were constructed by varying the concentration of each ion, both individually (with the other held constant) and simultaneously (with both ions present in the same solution), to evaluate the electrode's performance in mixed-ion systems. The PANI-modified PMBS biochar demonstrates significant potential for wastewater treatment and is suitable for a broader range of separation applications.

Introduction

The increasing contamination of water resources with heavy metal ions from industrial, mining, and agricultural activities has made the removal of these pollutants a critical environmental challenge.[1,2] Heavy metals, such as Pb, Cd, Hg, Cr, and Cu, pose a serious threat to human health and ecosystems owing to their high toxicity, long-term environmental persistence, and bioaccumulation potential.[3,4] These pollutants can enter the bodies of living organisms through the food chain, leading to various disorders, including neurological, renal, and hepatic impairments, as well as cancer.[5,6] Numerous methods have been developed for the removal of heavy metal ions from water, including adsorption,[7] ion exchange,[8] chemical precipitation,[9] membrane processes,[10] and electrochemical techniques.[11] Among these, adsorption has garnered significant attention owing to its high efficiency, low cost, operational simplicity, and potential for adsorbent regeneration.[12] Although traditional adsorbents such as activated carbon[13] and zeolites[14] are widely used, their high production costs and environmental concerns have driven researchers toward biochar derived from agricultural waste. Biochar, with its porous structure, large surface area, diverse functional groups, and low production costs, is considered a suitable alternative to commercial adsorbents.[15,16] Moreover, the use of agricultural waste for biochar production provides an effective solution for waste management and environmental pollution reduction.[17] Recently, the surface modification of biochar with nanoparticles and various functional groups has been explored to enhance its adsorption capacity and selectivity.[18] The optimization of operational conditions, such as pH, temperature, contact time, and initial pollutant concentration, also plays a crucial role in improving the removal efficiency of these contaminants.

[a]Department of Analytical Chemistry, Faculty of Chemistry and Petroleum Sciences, Bu-Ali Sina University, Hamedan, 6517838695, Iran. E-mail: afkhami@basu.ac.ir

[b]Department of Chemistry, College of Science, University of Sulaimani, Qlyasan Street, Sulaymaniyah City 46001, Kurdistan Region, Iraq. E-mail: kosar.hamaaziz@univsul.edu.iq

[c]Medical Laboratory Analysis Department, College of Health Sciences, Cihan University-Sulaimaniya, Sulaymaniyah 46001, Kurdistan Region, Iraq

† Electronic supplementary information (ESI) available. See DOI: https://doi.org/10.1039/d5ra02250a

Polyaniline (PANI), one of the most widely used conductive polymers, has attracted significant attention in various scientific and industrial fields owing to its unique physical and chemical properties.[19] This polymer exhibits high environmental stability, ease of synthesis, low cost, controllable electrical conductivity, and the ability to undergo oxidation state changes.[20] The unique molecular structure of polyaniline, which includes amine and imine functional groups, enables strong interactions with heavy metal ions through various mechanisms, such as complexation, ion exchange, and electrostatic attraction. Furthermore, the redox activity of polyaniline allows for the selective adsorption of metal ions at different pH levels.[21,22] Additionally, the structure of polyaniline can be modified through doping with acids, functionalization, and combination with other materials, such as nanoparticles, metal oxides, and carbon-based materials, which can enhance its adsorption properties and increase its adsorption capacity.[23] PANI is well known for enhancing adsorption properties owing to its high surface area, suitable porosity, and excellent chemical stability, making it an effective adsorbent for removing ionic pollutants from aqueous solutions.[24,25] Moreover, PANI exhibits good recyclability and reusability, which can be achieved through pH adjustments or electrochemical potential changes, thus offering an economical approach for water treatment applications.[26] Beyond adsorption, polyaniline has diverse applications in sensors, electronic devices, anti-corrosion coatings, and drug delivery systems, highlighting its potential for developing smart and multifunctional adsorbents for environmental pollutant removal.[27,28]

Magnetic adsorbents, a new generation of adsorbent materials, offer unique advantages in water treatment processes.[29,30] These adsorbents, typically composed of magnetic nanoparticles, such as Fe_3O_4 or γ-Fe_2O_3 combined with other adsorbent materials, enable rapid and easy separation from solutions using an external magnetic field. The integration of magnetic properties with the adsorption capabilities of various materials has led to the development of highly efficient hybrid adsorbents. For example, magnetic biochar, prepared through the pyrolysis of agricultural waste in the presence of iron nanoparticles, retains the advantages of biochar, such as its high surface area and diverse functional groups, while exhibiting magnetic separation capabilities.[31–33] The incorporation of magnetic components, such as iron oxides (e.g., Fe_3O_4), into biochar composites imparts magnetic properties to the material, enabling the facile separation and recovery of the adsorbent from aqueous solutions using an external magnetic field.[34] Magnetic biochar composites thus combine the high adsorption efficiency of biochar with the convenience of magnetic recyclability, making them promising candidates for sustainable and cost-effective water treatment technologies.[35] Moreover, magnetic modification can influence the surface charge and porosity of biochar, potentially enhancing the interaction between the adsorbent and target contaminants.[36] Additionally, the surface modification of magnetic adsorbents with polymers, such as polyaniline, can enhance the adsorption capacity, improve selectivity, and enable process control through pH or electrochemical potential adjustments. These magnetic hybrid adsorbents demonstrate high efficiency in removing heavy metal ions and reducing operational costs by eliminating the need for filtration or centrifugation. Furthermore, the recyclability and reusability of these adsorbents make them sustainable and economical options for industrial applications. Recent innovations in the synthesis of multifunctional and smart magnetic adsorbents have presented a promising outlook for the development of efficient water treatment systems.

In this study, for the first time, a novel magnetic bio-based adsorbent derived from sesame seed biochar and polyaniline was synthesized and applied for the removal of heavy metal ions, specifically mercury (Hg) and copper (Cu), from aqueous solutions. This hybrid adsorbent was prepared through the pyrolysis of sesame seeds, magnetization using $FeCl_3$, and subsequent surface modification with polyaniline. The unique combination of biochar properties (such as high surface area and diverse functional groups), magnetic separation capability, and adsorption characteristics of polyaniline (including amine and imine functional groups and redox activity) resulted in the development of an efficient, cost-effective, and environmentally friendly adsorbent. This innovative adsorbent not only utilizes agricultural waste but also enables rapid and easy separation from solutions owing to its magnetic properties, along with the potential for reuse. The present study aims to evaluate the efficiency of this adsorbent in removing Hg and Cu ions from aqueous solutions and to optimize the key parameters influencing the adsorption process. Additionally, square wave anodic stripping voltammetry (SWASV) was employed to measure the residual concentration of metal ions following the adsorption process.[37] Calibration curves for each ion were constructed both individually and simultaneously, and the corresponding graphs were included.

Materials and instrumentations

All chemicals used in this study were of analytical grade and were prepared using high-purity reagents. Iron(III) chloride hexahydrate ($FeCl_3 \cdot 6H_2O$) ($\geq$99%, Merck). Aniline ($\geq$99%, Merck), mercury(II) chloride ($HgCl_2$, 99%, Sigma-Aldrich), and copper(II) nitrate trihydrate ($Cu(NO_3)_2 \cdot 3H_2O$, analytical grade, Sigma-Aldrich) were used as received without further purification. The synthesized adsorbent was characterized using various analytical techniques: field emission scanning electron microscopy (FESEM) was performed using a JEOL JSM-6700 microscope; X-ray photoelectron spectroscopy (XPS) was conducted using a BesTek (Germany) X-ray photoelectron spectrometer; Brunauer–Emmett–Teller (BET) surface area analysis was carried out using a BELSORP MICU II from BEL Co.; magnetic properties were evaluated using a Lake Shore 7410 vibrating sample magnetometer (VSM); X-ray diffraction (XRD) analysis was performed using a PW1730 instrument from PHILIPS Co. with a 2θ range of 5–80°; centrifugation was performed using a centrifuge with a maximum rpm of 1300.

Preparation of biochar/Υ-Fe_2O_3 composite (MBS)

Initially, magnetic biochar (MBS) was synthesized from sesame seeds following a well-documented method in the literature.[38]
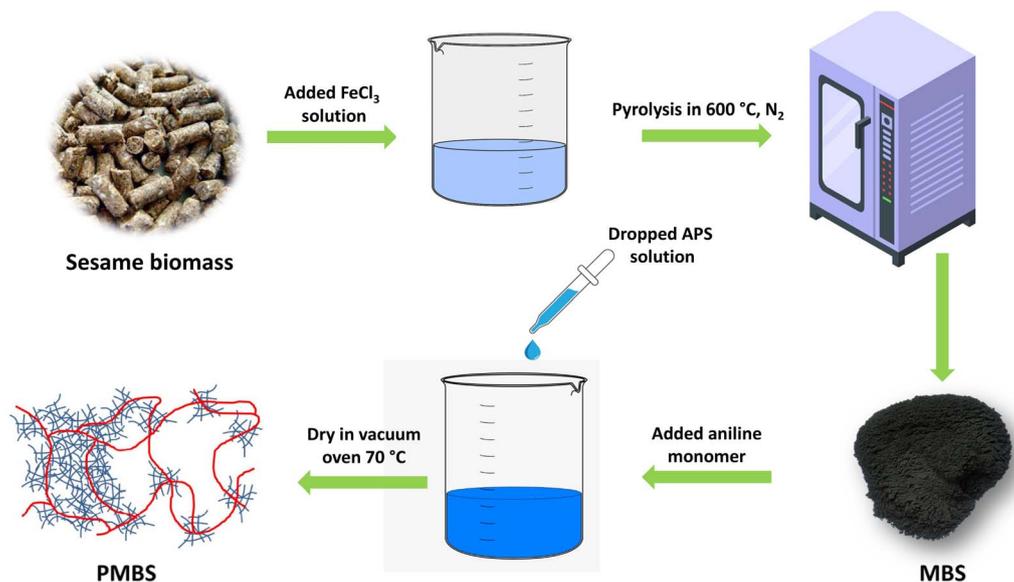
Fig. 1 Fabrication of PMBS.

The sesame seeds were first washed thoroughly to remove coarse impurities and then dried at 100 °C for 1 hour to eliminate residual moisture. To impart magnetic properties to the biochar, the dried seeds were immersed in a 1.0 M FeCl$_3$ solution for 24 hours, followed by another drying step. The resulting mixture was then subjected to pyrolysis in a vacuum furnace at 600 °C at a heating rate of 5 °C min^{-1} under a nitrogen (N$_2$) atmosphere for 4 hours. Finally, the obtained magnetic biochar was sieved through a 100-mesh screen to ensure uniform particle size for subsequent packaging and use (Fig. 1).

Preparation of PANI@Biochar/ϒ-Fe$_2$O$_3$ composite (PMBS)

To synthesize the polyaniline-modified magnetic biochar composite (PMBS), 2 g of pre-prepared magnetic biochar (MBS) was added to 100 mL of deionized water, and the mixture was stirred at room temperature for 30 minutes. Next, 5 mL of a 10 M hydrochloric acid (HCl) solution containing 0.1 mL of aniline was introduced into the above mixture, followed by vigorous stirring at room temperature for an additional 30 minutes. To initiate oxidative polymerization, 100 mL of a 10 M ammonium persulfate (APS) solution was added dropwise to the reaction mixture.[39] The polymerization reaction was carried out in an ice-water bath under continuous stirring for 5 hours. After the reaction was completed, the product was separated by an external magnetic field. The solid product was then washed several times with deionized water and ethanol to remove unreacted monomers and impurities. Finally, the obtained.

The PMBS composite was dried under vacuum at 70 °C for 12 hours (Fig. 1).

Optimization of PMBS synthesis

A critical aspect of the PMBS synthesis process is the optimization of the method to achieve the highest yield and performance of the composite. To this end, various ratios of magnetic

biochar (MBS) to aniline were mixed according to the synthesis method described above. Ultimately, different PMBS composites were synthesized with varying ratios of MBS to aniline. By evaluating the adsorption efficiency of the PMBS composites for Hg^{2+} and Cu^{2+} ions, it was determined that the composite with a 3 : 1 weight-to-weight (w/w) ratio of MBS to aniline exhibited the highest adsorption capacity (Fig. S1†). Further analysis revealed that increasing the aniline-to-MBS ratio led to a decrease in adsorption efficiency. This behavior is likely attributed to the blockage of pores on the adsorbent surface by excess aniline monomers, which can remain trapped in the structure and cavities of PMBS, thereby reducing its active surface area.

Conversely, a significant reduction in the amount of aniline can hinder the polymerization process, leading to insufficient functional groups on the adsorbent surface and a decrease in surface charge, which negatively impacts adsorption performance (Fig. S1†). Additionally, the adsorption capacities of raw biochar and MBS for Hg^{2+} and Cu^{2+} ions were investigated, and the results demonstrated that both exhibited significantly lower adsorption efficiencies compared to all synthesized PMBS composites (Fig. S1†). All adsorption experiments were conducted at room temperature and pH 6, and the results, expressed as percentages, were analyzed using the SWASV method and reported in the ESI File.†

Adsorption equilibrium

To conduct the adsorption equilibrium experiments, 10 mL of an aqueous solution containing Hg^{2+} and Cu^{2+} ions with an initial concentration of 30 mg L^{-1} was prepared. To each solution, 5 mg of PMBS was added as the adsorbent. The mixtures were then placed in a shaker at 150 rpm for 200 minutes at three temperatures (25 °C, 35 °C, and 45 °C). After reaching equilibrium, the concentration of the metal ions in the solution (C_e)

was measured. The equilibrium adsorption capacity, q_e (mg g^{-1}), was calculated using the following equation:

$$q_e = \frac{C_0 - C_e}{W} \times V,$$

where C_0, V, and W are the initial concentrations of metal ions (mg L^{-1}), solution volume (L), and the mass of the adsorbent (g), respectively. Additionally, the concentration of residual metal ions in the solution was evaluated using the SWASV technique.[37]

Adsorption kinetics

Adsorption kinetics experiments were conducted at pH values where the highest adsorption efficiencies were observed (pH = 6, 7, and 8). Similar to the equilibrium adsorption experiments, 5 mg of PMBS was added as the adsorbent to 10 mL of an aqueous solution containing Hg^{2+} and Cu^{2+} ions with an initial concentration of 30 mg L^{-1}. The mixtures were stirred at room temperature, and the samples were collected at specific time intervals to measure the residual concentration of metal ions (C_t). The amount of metal ions adsorbed at different pH values (q_t) was calculated using the following equation:

$$q_t = \frac{C_0 - C_t}{W} \times V,$$

The kinetics and equilibrium experiments were also performed repeatedly, and their error bars were reported. The concentration of residual metal ions in the solution was evaluated using the SWASV technique.[37]

Effect of pH on adsorption

To investigate the influence of pH on the removal of metal ions, aqueous solutions with pH values ranging from 2 to 11 were prepared using sodium hydroxide (NaOH) and hydrochloric acid (HCl). Following the same procedure as in previous experiments, 5 mg of PMBS was added as the adsorbent to 10 mL of an aqueous solution containing Hg^{2+} and Cu^{2+} ions

with an initial concentration of 30 mg L^{-1}. The mixtures were stirred at room temperature for 200 minutes. The initial and final concentrations of the metal ions were measured using the SWASV method. The percentage removal efficiency (%Re) of the metal ions was calculated using the following equation:

$$\%\text{Re} = \frac{A_0 - A}{A} \times 100,$$

where A_0 represents the initial concentration of the metal ion in solution before adsorption and A denotes the concentration after adsorption.

Results and discussion

PMBS is synthesized by the *in situ* oxidative polymerization of aniline in the presence of MBS, which facilitates strong interfacial bonding. PANI chains interact with hematite surfaces through hydrogen bonding and electrostatic interactions between the amine groups (–NH$_2$) of PANI and surface hydroxyl groups (–OH) of hematite. This interaction stabilizes the composite structure and maintains the magnetic properties essential for efficient adsorbent recovery. The crystalline structures of raw biochar, PMBS, PANI, and Υ-Fe$_2$O$_3$ were investigated using X-ray diffraction (XRD) analysis within the 2θ range of 10°–80° (Fig. 2A). As shown in the figure, no distinct diffraction peaks were observed for the raw biochar, indicating its amorphous nature. In contrast, the XRD pattern of Υ-Fe$_2$O$_3$ exhibited sharp peaks at $2\theta = 29.78°$, 36.24°, 45.67°, 52.18°, 55.36°, 61.89°, and 74.07°, corresponding to the crystalline planes (220), (311), (400), (422), (511), (440), and (533), respectively.[40] These peaks, which appeared with varying intensities, are characteristics of the cubic spinel structure of Υ-Fe$_2$O$_3$. The presence of these same peaks in the XRD pattern of PMBS confirms the successful incorporation of Υ-Fe$_2$O$_3$ into the synthesized adsorbent. Additionally, a broad peak was observed around $2\theta = 20°$ in the PMBS spectrum suggests the presence of polyaniline in the final composite structure, further supporting the successful modification of the biochar with both Υ-Fe$_2$O$_3$
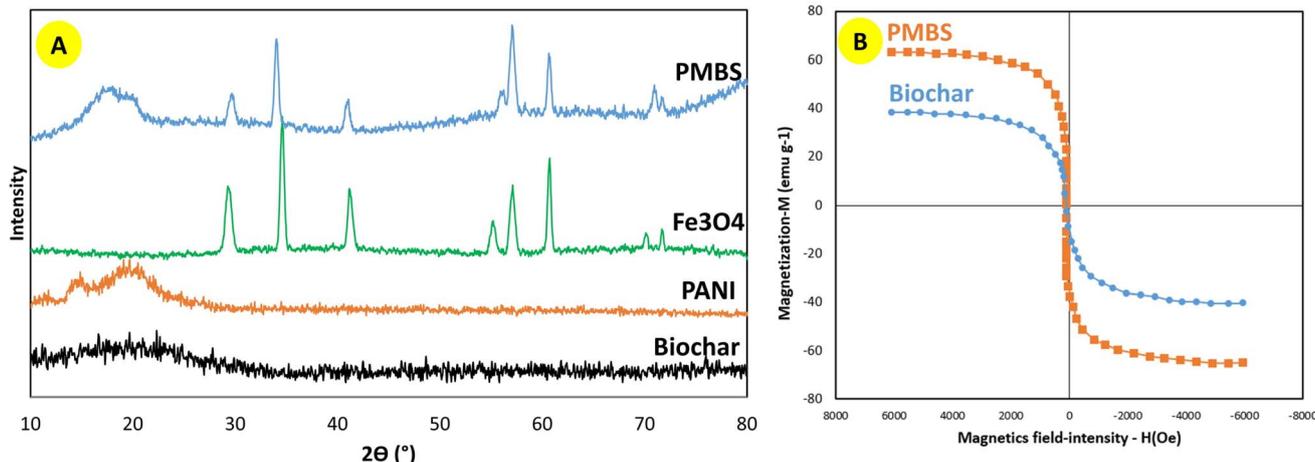

Fig. 2 (A) XRD patterns of biochar, PANI, γ-Fe$_2$O$_3$, and PMBS; (B) VSM analysis of PMBS.

and polyaniline. Fig. 2B presents the room-temperature magnetic hysteresis curves obtained from the vibrating sample magnetometer (VSM) analysis. The VSM analysis revealed that the saturation magnetization (M_s) of the MBC was higher than that of the PANI-modified magnetic biochar. This decrease in M_s after PANI coating can be attributed to the non-magnetic nature of polyaniline, which forms a protective layer around the magnetic Fe_3O_4 particles, partially shielding their magnetic response. Although the PMBS composite exhibits a reduced magnetic strength compared to pure MBS, its magnetization remains sufficient for magnetic separation using an external magnetic field. Moreover, the presence of PANI improves the surface functionality and adsorption performance of the composite.

To investigate pore size, pore volume, and surface area, BET analysis was employed. For this purpose, the results of the BET analysis for the MBS and PMBS compounds were compared (Fig. 3). The results indicate that the surface area of the PMBS compound is significantly larger than that of the MBS compound. The BET analysis revealed that the specific surface area of MBS compound increased from 152.01 $m^2 g^{-1}$ to 218.45 $m^2 g^{-1}$ after modification with polyaniline. Similarly, the total pore volume changed from 2.421 $cm^3 g^{-1}$ to 2.611 $cm^3 g^{-1}$.

These changes suggest that the polyaniline coating enhanced the porosity of the biochar matrix. The increase in surface area and pore volume is consistent with the observed improvement in adsorption capacity for Hg^{2+} and Cu^{2+} ions, as a higher surface area and appropriate pore structure facilitate better accessibility and more active sites for adsorption.

This increase in surface area could enhance the active sites available for the adsorption of metal contaminants. Furthermore, this analysis revealed that the pore volume and pore size of the PMBS compound are slightly larger than those of MBS, which may contribute to the physical adsorption of metal ions. However, it is important to note that the pore volume and size of PMBS are not substantially larger than those of MBS, suggesting that the significant factor enhancing adsorption is the chemical interaction of metal ions with functional groups on the surface, particularly the nitrogen groups in polyaniline. This indicates that the adsorption mechanism for heavy metals in PMBS is not solely dependent on the pore structure. Surface functional groups also play a crucial role in adsorption capacity.

The morphological and structural characteristics of the synthesized PMBS composite were examined using FE-SEM, as shown in Fig. 4. In Fig. 4A, the surface of the composite exhibits a rough and irregular morphology, with Fe_3O_4 nanoparticles
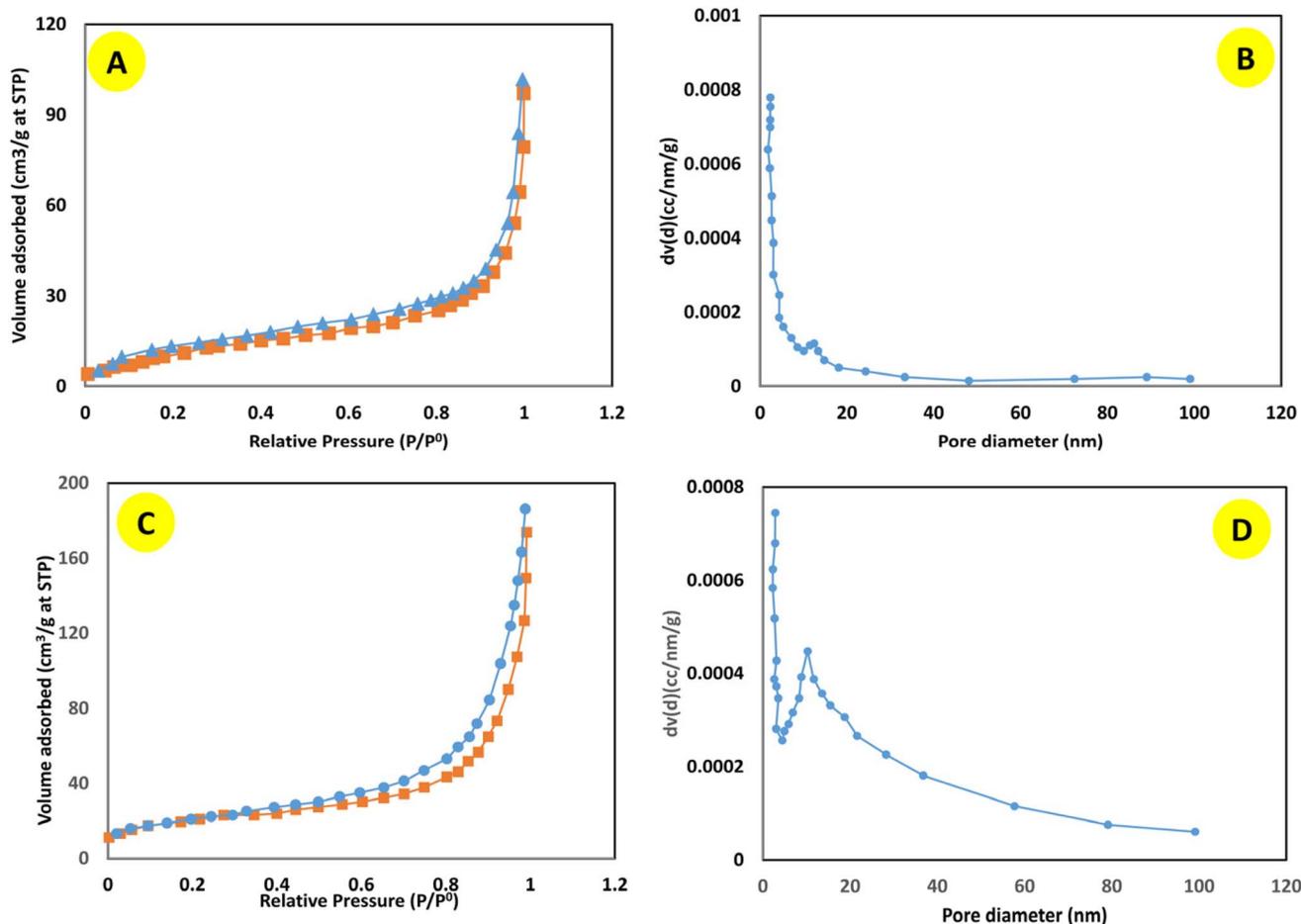

Fig. 3 Nitrogen adsorption–desorption isotherms and BJH pore-size distribution plots of (A and B) MBS and (C and D) PMBS.
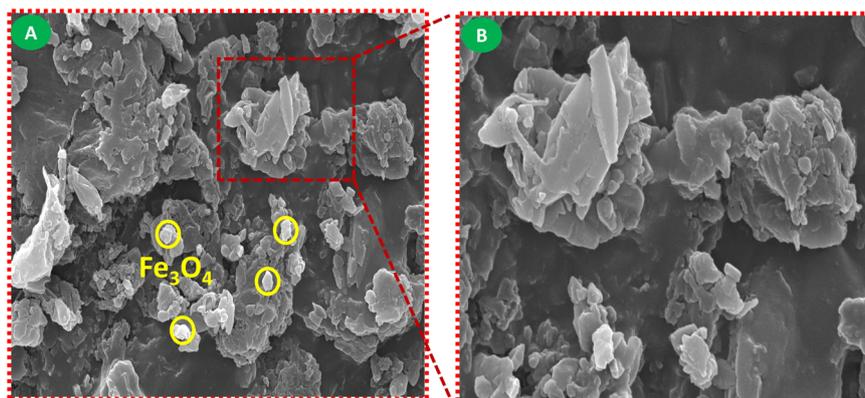
Fig. 4 FE-SEM images (A) PMBS and (B) magnified region.

clearly visible as bright-contrast spots (indicated in yellow circles). These particles are embedded within a polymer matrix and form cluster-like agglomerates resulting from the interaction with PANI during polymerization. Fig. 4B shows a magnified region, highlighting the heterogeneous distribution of plate-like and granular structures, which are typical of PMBS networks. The non-uniform dispersion of Fe_3O_4 throughout the composite contributes to its enhanced magnetic properties, which is consistent with the results obtained from XPS analysis.

X-ray photoelectron spectroscopy (XPS) analysis was conducted to examine the chemical interactions and electronic structure of the synthesized PMBS hybrid composite. As shown in Fig. 5, the XPS survey spectrum revealed four characteristic peaks corresponding to Fe 2p, O 1s, N 1s, and C 1s. High-resolution deconvolution of the C 1s spectrum displayed five distinct peaks at 282.5 eV (C=C), 283.4 eV (C–C/C–H), 284.5 eV (C–N/C=N), 285.9 eV (C=O), and 287.5 eV (C–N$^+$), demonstrating the diverse carbon bonding environments in the
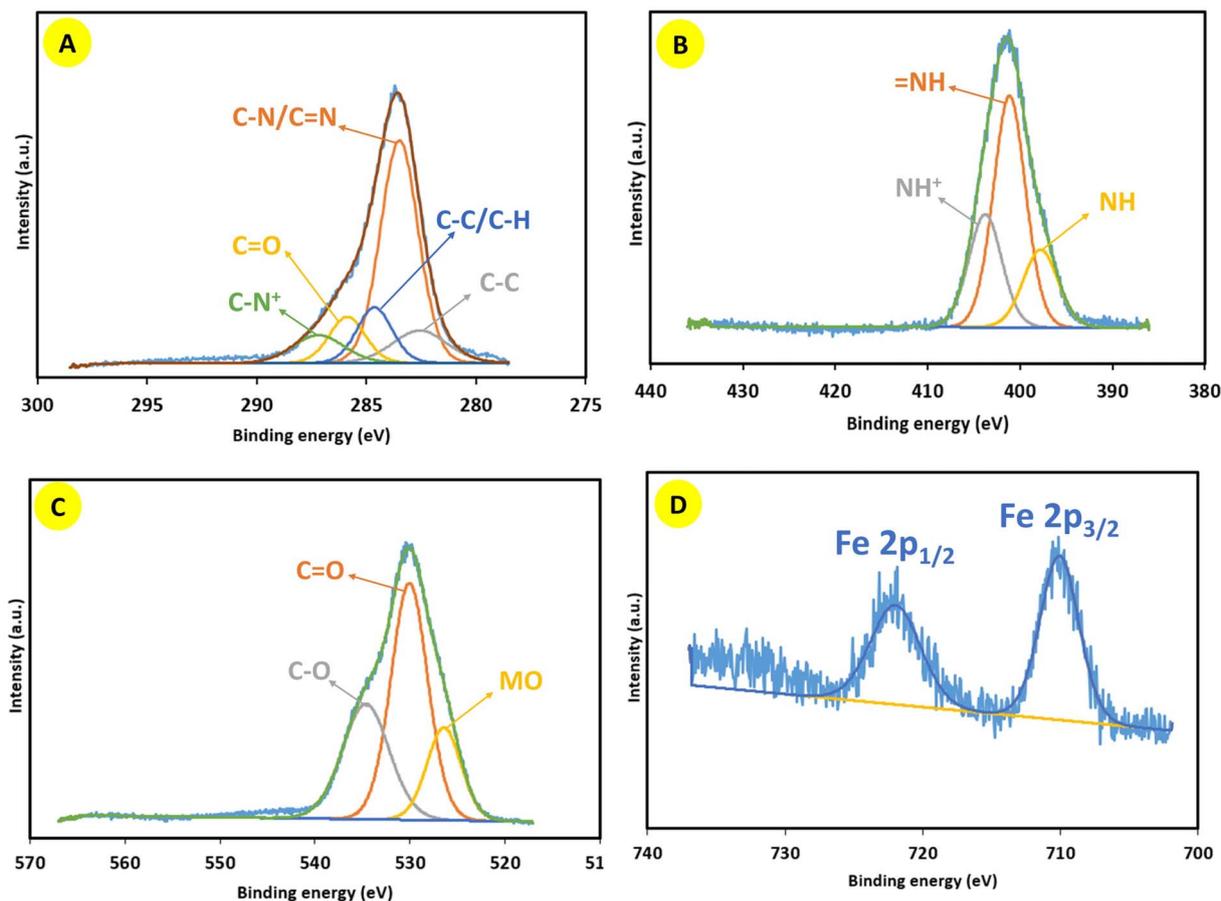

Fig. 5 XPS analyses of PMBS: (A) C 1s, (B) N 1s, (C) O 1s, and (D) Fe 2p.

composite. The N 1s spectrum was fitted with three Gaussian peaks at 396.6 eV (–NH–), 401.1 eV (=NH–), and 403.7 eV (–NH$^+$–), confirming the presence of polyaniline in various protonation states. The enhanced adsorption performance of PMBS can be related to the nitrogen-containing functional groups introduced by PANI. These nitrogen functionalities originate from the polyaniline coating and are known to possess lone pair electrons capable of coordinating with metal ions. The presence of these groups on the adsorbent surface suggests potential active sites for binding Hg^{2+} and Cu^{2+} ions through coordination bonds or electrostatic interactions. Although XPS analysis after adsorption was not performed, the identified nitrogen species strongly indicate their involvement in metal ion capture, consistent with previously reported mechanisms in similar polyaniline-based adsorbents.[41–43] The O 1s spectrum exhibited three components at 526.6 eV (metal–oxygen bonds), 531.1 eV (C=O), and 534.8 eV (C–O), with additional intensity suggesting abundant hydroxyl groups that may facilitate hydrogen bonding between MBS and PANI through electron cloud interactions. Finally, the Fe 2p spectrum showed characteristic spin–orbit doublets at 710.9 eV (Fe 2p$_{3/2}$) and 722.2 eV (Fe 2p$_{1/2}$), consistent with Fe^{3+} in Fe$_3$O$_4$, with no detectable Fe^{2+} impurities, confirming the phase purity of the magnetic component. These results collectively verify the successful formation of the PMBS hybrid composite and highlight the critical role of surface functional groups in mediating interfacial interactions.

Adsorption isotherm

An adsorption isotherm describes the relationship between the amount of a substance adsorbed onto the surface of an adsorbent and its pressure or concentration in the gas or liquid phase at a constant temperature. It provides insight into how the adsorbate is adsorbed by the adsorbent and aids in understanding adsorption behavior and designing adsorption systems. Specifically, an adsorption isotherm represents the relationship between the amount of metal ions adsorbed at equilibrium (q_e) and the remaining concentration (C_e) at a constant temperature. Adsorption equilibrium experiments for Hg^{2+} and Cu^{2+} ions were conducted at three temperatures

(25, 35, and 45 °C). The results are illustrated in Fig. 6. It is evident that, at all temperatures, the adsorption capacity increases as the temperature increases and eventually reaches a saturation point. This behavior highlights the temperature-dependent nature of the adsorption process and the attainment of equilibrium under the given experimental conditions.

Several factors can explain the increase in adsorption capacity with increasing temperature. One of these reasons is the enhancement of the chemisorption processes. Unlike physisorption, which relies on weak van der Waals or electrostatic forces, chemisorption requires activation energy and is typically irreversible.[44] As the temperature increases, the necessary energy for forming these chemical bonds is provided, leading to an increase in the adsorption rate and the number of active sites on the adsorbent that interact with metal ions.[45] This phenomenon results in a higher adsorption capacity in chemisorption processes as the temperature increases. Another reason could be the increased mobility of ions, which is a significant factor in the enhanced adsorption of metal ions, such as Hg^{2+} and Cu^{2+}, at higher temperatures.[46] As the temperature increases, the kinetic energy of the ions increases, causing them to move more rapidly in the solution. This enhanced mobility allows the ions to reach the adsorbent surface more quickly and interact with the active sites on the adsorbent. Additionally, higher temperatures may reduce inhibitory effects, such as boundary layer resistance,[47] which typically reduces the movement of ions toward the adsorbent surface. By minimizing these barriers, mass transfer is improved, and ions can more easily access the adsorbent surface. Consequently, the likelihood of collisions and adsorption of ions by the active sites increases, leading to a higher adsorption capacity. This phenomenon is particularly significant in systems where adsorption is diffusion-controlled. In summary, the increase in adsorption capacity with temperature can be attributed to the promotion of chemisorption processes, enhanced ion mobility, and reduced mass transfer limitations, all of which contribute to more efficient interactions between metal ions and the adsorbent surface. Based on the observations, it can be concluded that the adsorption process of Hg^{2+} and Cu^{2+} ions by the synthesized PMBS adsorbent is
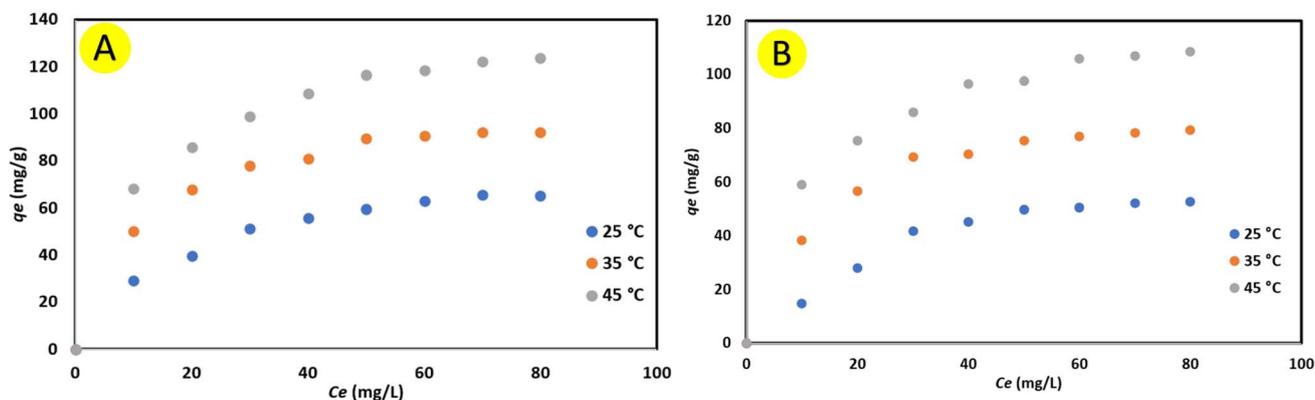

Fig. 6 Curve of the adsorption isotherm of (A) Hg^{2+} and (B) Cu^{2+} at different temperatures.

endothermic. In other words, an increase in temperature, according to Le Chatelier's principle, shifts the equilibrium toward increased adsorption.[48] In this case, the adsorption equilibrium constant (K) increases with temperature, leading to the enhanced adsorption of metal ions, such as Hg^{2+} and Cu^{2+}.

To evaluate the behavior of the PMBS adsorbent in equilibrium experiments, the results were compared with two-parameter isotherm models, namely the Langmuir[49] and Freundlich[50] models, using a nonlinear regression approach.[51]

The Langmuir equation is a theoretical model used to describe monolayer adsorption on a homogeneous adsorbent surface.[49] This equation is based on three main assumptions: (1) adsorption occurs at specific finite sites on the adsorbent surface; (2) each site can adsorb only one molecule or ion; and (3) all sites have the same adsorption energy, and there are no interactions between adsorbed molecules. In contrast, the Freundlich equation is an empirical model used to describe adsorption on heterogeneous surfaces.[52] This equation applies to systems in which adsorption occurs in multilayers or in which adsorption sites have varying energies.

To determine the best fit, the values of the root mean square error (RMS) and the coefficient of determination (R^2) were evaluated. By analyzing these parameters, and considering that a closer R^2 value to 1 and a lower RMS indicate a better fit, it was found that the Langmuir isotherm exhibited the highest correlation with the results obtained from the equilibrium experiments (Tables 1, 2 and S1–S4†). The alignment with the Langmuir isotherm model suggests that the active sites on the PMBS surface are homogeneously distributed and uniformly accessible throughout the adsorbent material. Additionally, each site can adsorb only one molecule or ion.

Furthermore, by comparing the q_{max} (maximum adsorption capacity) and K_L (Langmuir constant) for the adsorption of the two metal ions, Cu^{2+} and Hg^{2+}, it was observed that PMBS has a greater affinity for adsorbing Hg^{2+} compared to Cu^{2+}. Since a smaller ionic radius increases the tendency of an ion to undergo hydrolysis, the Cu^{2+} ion has a higher tendency to hydrolyze, making it less available for adsorption.[53] In contrast, Hg^{2+}, with its larger ionic radius, is less prone to hydrolysis and more readily adsorbed by the PMBS adsorbent.

However, the Freundlich isotherm showed a weaker correlation with the experimental results. Although the Langmuir

isotherm provided a better fit to the experimental data, the RMSE and R^2 values for the Freundlich model were still reasonable (Tables 2, 3 and S1–S4†). However, the relatively low coefficient of determination and high $1/n$ values obtained from fitting the experimental data to the Freundlich equation suggest a weaker adsorption intensity although they do not necessarily invalidate the model. These results indicate that the Freundlich model may be less appropriate for describing the adsorption process under the given conditions.

In summary, by comparing the values of $1/n$ and the coefficient of determination (R^2) obtained for each isotherm model, the order of fit is as follows: Langmuir > Freundlich. This conclusion highlights the homogeneous nature of the adsorption sites on the PMBS surface and the monolayer adsorption mechanism, as described by the Langmuir model, which aligns well with the experimental observations. Although the adsorption is predominantly described by the Langmuir model, indicating monolayer adsorption, the presence of polar nitrogen-containing groups and the conjugated π-electron system in PANI suggests that chemisorption may also play a role. Coordination bonding between metal ions and nitrogen functionalities, as well as π–cation interactions, could contribute to the adsorption process. This implies a mixed adsorption mechanism involving both physical adsorption (electrostatic attraction and van der Waals forces) and chemical interactions (chemisorption). Such mixed mechanisms are often reflected in minor deviations from ideal isotherm fitting, as observed in our kinetic and isotherm analyses.

Finally, the adsorption process on PMBS likely involves multiple mechanisms: (i) electrostatic attraction between negatively charged surface groups and metal cations, (ii) coordination bonding *via* nitrogen functionalities acting as chelating sites, (iii) π–cation interactions from the conjugated polymer matrix, and (iv) pore diffusion within the biochar matrix enhancing accessibility of active sites. This multifaceted adsorption mechanism contributes to the high efficiency and selectivity of PMBS toward Hg^{2+} and Cu^{2+} ions in aqueous solutions.

Effect of pH

In general, the pH of an aqueous solution is one of the most critical factors influencing the adsorption of heavy metals.[54] Typically, the adsorption of heavy metals increases at higher pH values (alkaline conditions), whereas it decreases at lower pH values (acidic conditions). However, this behavior can vary depending on the type of metal and the adsorbent used. Therefore, optimizing the pH is essential for maximizing the adsorption of heavy metals in water and wastewater treatment systems. Consequently, determining the optimal pH for the

Table 1 Surface area, pore volume, and pore size of MBS and PMBS

Samples	BET-SSA ($m^2\ g^{-1}$)	Total pore volume ($cm^3\ g^{-1}$)	Average pore diameter (nm)
MBS	218.45	2.611	0.48
PMBS	152.01	2.421	0.64

Table 2 Isotherm model parameters for the adsorption of Hg^{2+} on PMBS at 45 °C

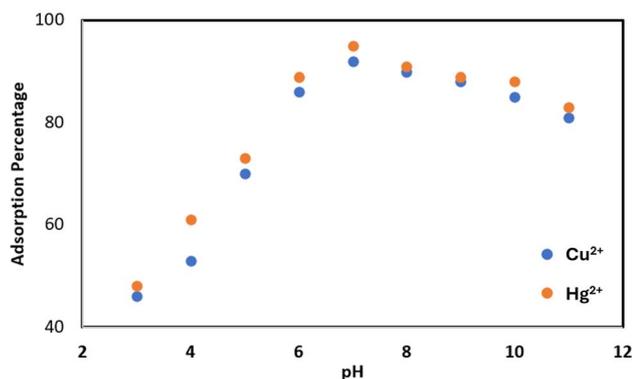| Isotherm model	q_{max} (mg g^{-1})	K_L (L mg^{-1})	K_F (L $mg^{(1-(1/n))}\ g^{-1}$)	$1/n$	RMS	r^2
Langmuir	141.8947	0.0838	—	—	2.218439	0.997261
Freundlich	—	—	37.5996	0.2795	3.012418	0.994949

Table 3 Isotherm model parameters for the adsorption of Cu^{2+} on PMBS at 45 °C

Isotherm model	q_m (mg g^{-1})	K_L (L mg^{-1})	K_F (L mg$^{(1-(1/n))}$ g^{-1})	$1/n$	RMS	r^2
Langmuir	124.7892	0.0812	—	—	2.138874	0.996687
Freundlich	—	—	32.1196	0.2853	2.725436	0.994621

Fig. 7 Effect of pH$_i$ on the adsorption process.

adsorption of metal contaminants is of great importance. To investigate the effect of pH on the removal of metal ions, the initial pH (pH$_i$) of the solution was adjusted using HCl and NaOH in the range of 3–11, and the adsorption capacity of each ion was measured at different pH values (Fig. 7). The experimental results indicate that the adsorption of Cu^{2+} and Hg^{2+} ions by the synthesized adsorbent (PMBS) reaches its maximum at pH = 7 and decreases as the pH deviates from this value. This behavior can be explained by considering the influence of pH on the surface charge of the adsorbent, the chemical speciation of the metals, and ionic competition.

At low pH (acidic conditions, pH < 7), the high concentration of H$^+$ ions in the solution leads to competition between these ions and Cu^{2+} and Hg^{2+} ions for adsorption sites on the adsorbent surface.[55] Since H$^+$ ions are smaller and more mobile, they readily occupy the adsorption sites, resulting in the reduced adsorption of heavy metal ions. Additionally, at a very low pH, the functional groups on the adsorbent surface may become protonated and acquire a positive charge, leading to electrostatic repulsion between the adsorbent and the positively charged metal ions (Cu^{2+} and Hg^{2+}), which further reduces adsorption.[56] As the pH approaches neutral conditions (pH ≈ 7), the concentration of H$^+$ ions decreases, reducing their competition with metal ions for active adsorption sites. In this pH range, functional groups on the adsorbent surface may partially or fully deprotonate, resulting in a negatively charged surface that enhances the adsorption of positively charged Cu^{2+} and Hg^{2+} ions *via* electrostatic attraction.[57] With a further increase in pH towards alkaline conditions (pH > 7), although adsorption remains relatively high, a slight decrease in adsorption is observed. This reduction may be attributed to the formation of metal hydroxide complexes (such as $Cu(OH)_2$ and $Hg(OH)_2$). As the probability of forming low-solubility metal

hydroxides increases, the likelihood of metal adsorption by the adsorbent decreases. However, these compounds can physically precipitate onto the adsorbent surface and enhance adsorption. Therefore, adsorption did not decrease significantly. Additionally, at very high pH values, the functional groups on the adsorbent surface may become fully deprotonated, resulting in a strongly negative surface charge. Under these conditions, metal ions may form insoluble hydroxide precipitates or negatively charged complexes, leading to reduced adsorption due to electrostatic repulsion between the adsorbent and the metal complex ion species. Overall, the adsorption behavior of Cu^{2+} and Hg^{2+} by the PMBS adsorbent demonstrates a complex equilibrium between various factors, such as adsorbent surface charge, chemical speciation of metals, and ionic competition, all of which are influenced by pH. In summary, this study highlights the vital role of solution pH in the adsorption of Hg^{2+} and Cu^{2+} onto PMBS. The optimal pH for maximum removal of these metal ions is between pH 6 and pH 8, where more than 90 percent removal is achieved.

Adsorption kinetics

The next stage in the adsorption process is to examine the kinetics of adsorption, which can provide valuable insights into adsorption mechanisms, such as mass transfer and chemical reactions from aqueous solutions. Experimental data from equilibrium kinetic experiments for Hg^{2+} and Cu^{2+} metal ions over a time range of 0–200 minutes at varying pH values of 6–8 (pH levels where maximum adsorption occurred) were analyzed (Fig. 8). As expected, the results showed that adsorption capacity highly depends on both initial pH and time. At pH values lower and higher than 7, a decrease in adsorption capacity was observed; the reasons for this were explained in the previous section. The decrease in adsorption was attributed to the protonation of the active sites on the PMBS surface. Conversely, at pH 6, where active sites become protonated, the adsorption capacity of metal ions increases significantly owing to enhanced ion adsorption. However, at higher pH levels, the presence of hydroxide ions and the hydration of metal ions lead to reduced adsorption efficiency. Consequently, the rate of adsorption decreases until equilibrium is achieved. This investigation also showed that the adsorption process typically reaches equilibrium within the first 160 minutes.

To investigate the adsorption mechanism, the obtained kinetic data were fitted using two kinetic models: pseudo-first-order (PFO) and pseudo-second-order (PSO) models. Kinetic parameters, root mean square error (RMS) values, and correlation coefficients (R^2) for both models were determined using nonlinear curve fitting analysis with nonlinear least squares regression (curve fitter).
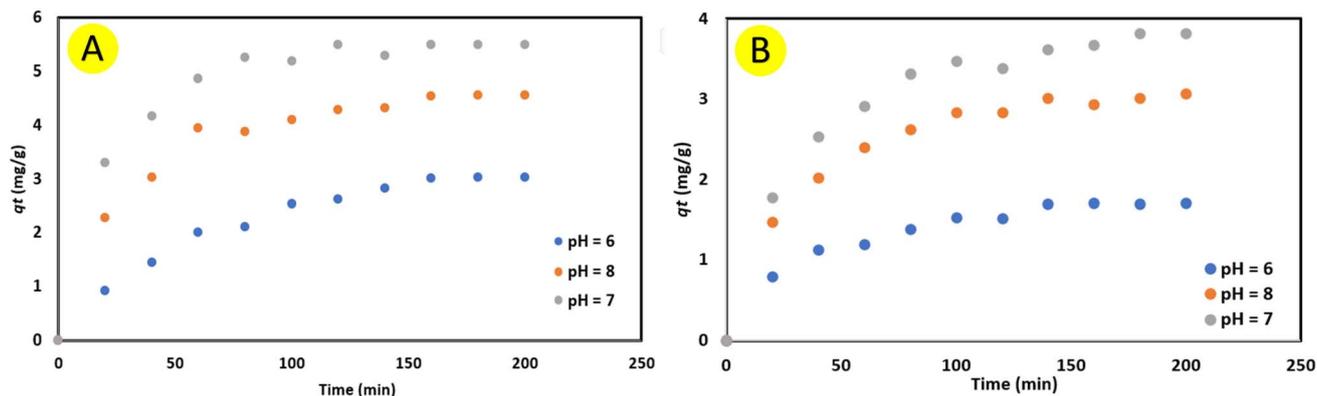
Fig. 8 Experimental kinetic data for the adsorption of (A) Hg^{2+} and (B) Cu^{2+} on PMBS.

Table 4 Calculated kinetics model parameters for the adsorption of Cu^{2+} and Hg^{2+} on CMBA at pH 7

Kinetic model	q_e (mg g^{-1})	k_1 (1/s)	k_2 (g mg^{-1} s^{-1})	RMS	R^2
Hg^{2+}					
PFO	5.4228	0.0412	—	0.145348	0.993101
PSO	6.0575	—	0.0101	0.124082	0.994972
Cu^{2+}					
PFO	3.7095	0.0285	—	0.114676	0.991116
PSO	4.3711	—	0.0080	0.065864	0.997069

The analysis of Hg^{2+} and Cu^{2+} adsorption data by the PMBS adsorbent revealed that the PSO kinetic model provided the best fit to the experimental data (Tables 4, S5, and S6†). The PFO model, which is based on simpler assumptions, such as the linear dependence of adsorption on time, failed to adequately describe adsorption behavior in the studied system. This was evident through the significant deviation between the equilibrium adsorption capacity (q_e) values calculated by the PFO model and the experimental values. Additionally, the PFO model showed lower R^2 values and higher RMS values, indicating insufficient agreement between this model and the experimental data. These deviations may result from the PFO model's neglect of more complex factors affecting the adsorption process, such as chemical and physical interactions between the adsorbent and metal ions.

In contrast, the PSO model, which is based on more complex and realistic assumptions, such as the nonlinear dependence of adsorption on time and the influence of metal ion concentration on adsorption rate, demonstrated a much better fit for the experimental data. The q_e values calculated by the PSO model were significantly closer to the experimental values. Furthermore, the higher R^2 values and lower RMS values obtained from this model indicate a closer alignment between the model predictions and experimental data. These results suggest that the PSO model can more accurately describe the mechanisms of Hg^{2+} and Cu^{2+} adsorption in the studied system. These mechanisms likely involve stronger chemical interactions, such as the formation of covalent bonds or surface complexes between metal ions and functional groups on the surface of the PMBS

adsorbent. Additionally, the PSO model may better account for the influence of other factors, such as ionic competition and the saturation of adsorption sites in the adsorption process.

Additionally, the rate constant (k) obtained from the PSO model shows an increasing trend with increasing initial solution pH, which aligns well with the experimental data. These findings indicate that the deprotonation of active sites on the adsorbent surface at higher pH values plays a key role in enhancing adsorption interactions and improving the performance of the PMBS adsorbent. Consequently, the adsorption rate increases, and the overall efficiency of the adsorption process improves significantly. In summary, the increase in rate constant (k) with increasing initial pH, along with its precise alignment with experimental data, confirms that pH is one of the most important factors controlling adsorption mechanisms in adsorbent-metal systems. These results not only provide a better understanding of the behavior of the PMBS adsorbent in removing heavy metals but also highlight the importance of pH optimization in the design and application of adsorbents for water and wastewater treatment.

Additionally, the adsorption capacity of the PMBS adsorbent for removing Hg^{2+} and Cu^{2+} ions from aqueous solutions was compared with results reported for other adsorbents in previous studies (Table 5). The q_{max} values (maximum equilibrium adsorption capacity) for PMBS were determined to be 141.89 mg g^{-1} for Hg^{2+} and 124.78 mg g^{-1} for Cu^{2+}. These values are higher compared to many bio-based or chemically synthesized adsorbents reported in the scientific literature. These findings indicate that PMBS possesses a higher adsorption capacity and can

Table 5 Adsorption capacity of Hg^{2+} and Cu^{2+} by different bio-based adsorbents

Adsorbent	Hg^{2+} (mg g^{-1})	Cu^{2+} (mg g^{-1})	Ref.
Activated biochar	—	17.25	58
Coconut-derived activated carbon	—	73.60	59
Modified pine sawdust	—	101.6	60
Magnetic chitosan-phenylthiourea	135.08	—	61
Thiol-functionalized-zeolite	89.31	—	62
$Fe_3O_4@SiO_2$-SH nanoparticles	132.11	—	63
PMBS	141.89	124.78	This work

be used as an effective and efficient material for removing heavy metals from aqueous environments.

To evaluate the practical applicability of PMBS, reusability tests were performed over five consecutive adsorption–desorption cycles. The adsorbent was regenerated using a mild acidic solution (0.1 M HCl) and tested under identical conditions to assess its performance. The results demonstrated a slight decrease in adsorption performance after five cycles, from 95% to 87% for Hg^{2+} and from 91% to 82% for Cu^{2+}, indicating a minimal loss in adsorption capacity. This suggests good stability and reusability of the adsorbent likely owing to the limited degradation of active sites (Fig. S4†). The observed decline in efficiency may be attributed to minor structural changes or incomplete desorption. Additionally, the magnetic properties of the PMBS adsorbent remained stable after five cycles. These findings highlight the potential of the synthesized adsorbent for long-term application in wastewater treatment, supporting its economic and operational viability. Further studies are recommended to optimize regeneration protocols and improve recovery efficiency. The improved performance of the modified PMBS can be attributed to several key factors. First, the larger active surface area of this adsorbent increases the number of available adsorption sites for metal ions, which directly affects the adsorption capacity. Second, stronger interactions between heavy metal ions and functional groups on the PMBS surface (such as hydroxyl, carboxyl, and amino groups) enhance the adsorbent's affinity for metal ions. These interactions can include the formation of covalent bonds, surface complexes, and electrostatic attractions. Third, the biological composition of PMBS represents an important environmental advantage, as this adsorbent is made from natural or biodegradable materials and consequently does not produce any hazardous by-products or secondary pollutants. This characteristic makes PMBS an environmentally friendly option that can minimize negative effects on ecosystems.

Another prominent advantage of PMBS is its magnetic property, which enables easy and rapid separation of the adsorbent from the aqueous environment after the adsorption process. This feature is particularly valuable in practical applications, such as water and wastewater treatment, as it eliminates the need for complex and time-consuming separation processes, such as filtration or centrifugation. By applying an external magnetic field, the magnetic PMBS adsorbent is easily separated from the aqueous environment, which increases the efficiency of the process and reduces operational costs. This magnetic property, combined with its high adsorption capacity and environmental compatibility, makes PMBS an ideal adsorbent for industrial use.

Conclusion

In this study, the synthesis of magnetic biochar modified with the organic material polyaniline (PANI) derived from sesame seed cake (PMBS) was demonstrated to be an effective biosorbent. The PMBS composite was obtained using sesame seed waste, which is abundant and inexpensive in our country and is considered unused waste. The synthesis of this composite can be regarded as a green chemistry approach because it does not produce any harmful by-products for the environment and is biodegradable. The synthesized PMBS composite was used as an effective adsorbent for the removal of Hg^{2+} and Cu^{2+} from aqueous solutions. The experimental data were analyzed using both kinetic and equilibrium models. The evaluation revealed that the adsorption behavior of the synthesized adsorbent for heavy metal removal is closer to the pseudo-second-order kinetic model. Additionally, the equilibrium data fit well with the Langmuir isotherm model, indicating homogeneous adsorption sites on the PMBS surface. Finally, by comparing the adsorption capacity of the synthesized PMBS adsorbent with that reported in the literature, the superior performance of PMBS in heavy metal adsorption was confirmed. The bio-based nature, simple and cost-effective synthesis method, biodegradability, and excellent adsorption performance of PMBS highlight its potential for industrial applications in the removal of metal ions from aqueous solutions. These characteristics position PMBS as a promising candidate for sustainable and efficient water purification technologies.

Data availability

Data availability is not applicable to this article as no new data were created or analyzed in this study.

Conflicts of interest

The authors have no conflicts of interest to declare.

References

1 A. H. Jagaba, I. M. Lawal, A. H. Birniwa, A. C. Affam, A. K. Usman, U. B. Soja, D. Saleh, A. Hussaini, A. Noor and N. S. A. Yaro, in *Membrane Technologies for Heavy Metal Removal from Water*, CRC Press, 2024, pp. 3–27.

2 G. Tripathi, A. Husain, S. Ahmad, Z. Hasan and A. Farooqui, in *Contamination of Water*, Elsevier, 2021, pp. 85–98.

3 A. Singh, A. Sharma, R. K. Verma, R. L. Chopade, P. P. Pandit, V. Nagar, V. Aseri, S. K. Choudhary, G. Awasthi and K. K. Awasthi, in *The Toxicity of Environmental Pollutants*, IntechOpen, 2022.

4 K. H. H. Aziz, F. S. Mustafa, K. M. Omer, S. Hama, R. F. Hamarawf and K. O. Rahman, *RSC Adv.*, 2023, **13**, 17595–17610.

5 K. Sardar, S. Ali, S. Hameed, S. Afzal, S. Fatima, M. B. Shakoor, S. A. Bharwana and H. M. Tauqeer, *GJEMPS*, 2013, **2**, 172–179.

6 K. H. H. Aziz, F. S. Mustafa, R. F. Hamarawf and K. M. Omer, *J. Water Process Eng.*, 2025, **70**, 106867.

7 M. Z. A. Zaimee, M. S. Sarjadi and M. L. Rahman, *Water*, 2021, **13**, 2659.

8 A. Bashir, L. A. Malik, S. Ahad, T. Manzoor, M. A. Bhat, G. Dar and A. H. Pandith, *Environ. Chem. Lett.*, 2019, **17**, 729–754.

9 A. Pohl, *Water, Air, Soil Pollut.*, 2020, **231**, 503.

10 H. A. Qdais and H. Moussa, *Desalination*, 2004, **164**, 105–110.

11 C. Liu, T. Wu, P.-C. Hsu, J. Xie, J. Zhao, K. Liu, J. Sun, J. Xu, J. Tang and Z. Ye, *ACS Nano*, 2019, **13**, 6431–6437.

12 R. Chakraborty, A. Asthana, A. K. Singh, B. Jain and A. B. H. Susan, *Int. J. Environ. Anal. Chem.*, 2022, **102**, 342–379.

13 M. Raninga, A. Mudgal, V. K. Patel, J. Patel and M. K. Sinha, *Mater. Today: Proc.*, 2023, **77**, 286–294.

14 E. Pérez-Botella, S. Valencia and F. Rey, *Chem. Rev.*, 2022, **122**, 17647–17695.

15 K. H. H. Aziz and R. Kareem, *Case Stud. Chem. Environ. Eng.*, 2023, **8**, 100495.

16 K. H. H. Aziz, F. S. Mustafa, M. A. Hassan, K. M. Omer and S. Hama, *Desalination*, 2024, 117725.

17 M. A. Karim and K. H. H. Aziz, *J. Water Process Eng.*, 2025, **75**, 108014.

18 M. Zahedifar, N. Seyedi, S. Shafiei and M. Basij, *Mater. Chem. Phys.*, 2021, **271**, 124860.

19 Z. A. Boeva and V. G. Sergeyev, *Polym. Sci., Ser. C*, 2014, **56**, 144–153.

20 M. Jaymand, *Prog. Polym. Sci.*, 2013, **38**, 1287–1306.

21 M. Higuchi, D. Imoda and T. Hirao, *Macromolecules*, 1996, **29**, 8277–8279.

22 N. Gospodinova, V. Muşat, H. Kolev and J. Romanova, *Synth. Met.*, 2011, **161**, 2510–2513.

23 G. Liao, Q. Li and Z. Xu, *Prog. Org. Coat.*, 2019, **126**, 35–43.

24 J. Stejskal and R. Gilbert, *Pure Appl. Chem.*, 2002, **74**, 857–867.

25 R. Bushra, M. Shahadat, M. Khan, R. Adnan, M. Arshad, M. Rafatullah and M. Naushad, *Int. J. Environ. Sci. Technol.*, 2015, **12**, 3635–3642.

26 B. Ou, J. Wang, Y. Wu, S. Zhao and Z. Wang, *Chemosphere*, 2020, **245**, 125689.

27 H. Bai and G. Shi, *Sensors*, 2007, **7**, 267–307.

28 P. Najmi, N. Keshmiri, M. Ramezanzadeh and B. Ramezanzadeh, *Chem. Eng. J.*, 2021, **412**, 128637.

29 O. V. Kharissova, H. R. Dias and B. I. Kharisov, *RSC Adv.*, 2015, **5**, 6695–6719.

30 A. Sharma, D. Mangla and S. A. Chaudhry, *J. Environ. Manage.*, 2022, **306**, 114483.

31 Y. Yi, Z. Huang, B. Lu, J. Xian, E. P. Tsang, W. Cheng, J. Fang and Z. Fang, *Bioresour. Technol.*, 2020, **298**, 122468.

32 J. Qu, J. Shi, Y. Wang, H. Tong, Y. Zhu, L. Xu, Y. Wang, B. Zhang, Y. Tao and X. Dai, *J. Hazard. Mater.*, 2022, **434**, 128841.

33 Y. Li, J. Zhang, D. Cheng, W. Guo, H. Liu, A. Guo, X. Chen, Y. Wang and H. H. Ngo, *J. Environ. Manage.*, 2024, **366**, 121872.

34 B. Chen, Z. Chen and S. Lv, *Bioresour. Technol.*, 2011, **102**, 716–723.

35 Q. Zhao, T. Xu, X. Song, S. Nie, S.-E. Choi and C. Si, *Front. Bioeng. Biotechnol.*, 2021, **9**, 769667.

36 J. Wang and M. Zhang, *Int. J. Environ. Res. Public Health*, 2020, **17**, 1075.

37 S. A. Kitte, S. Li, A. Nsabimana, W. Gao, J. Lai, Z. Liu and G. Xu, *Talanta*, 2019, **191**, 485–490.

38 D. H. K. Reddy and S.-M. Lee, *Colloids Surf., A*, 2014, **454**, 96–103.

39 X. Zheng, M. Ali Mohsin, A. Arsad and A. Hassan, *J. Appl. Polym. Sci.*, 2021, **138**, 50637.

40 Y.-q. Wang, K. Li, M.-y. Shang, Y.-z. Zhang, Y. Zhang, B.-l. Li, Y.-j. Kan, X.-q. Cao and J. Zhang, *Chem. Eng. J.*, 2023, **451**, 138655.

41 B. Shi, H. Li, X. Fu, C. Zhao, A. H. Wang, W. Tan, Y. Rao, M. Li, S. Komarneni and H. Yang, *Sep. Purif. Technol.*, 2024, **335**, 125866.

42 J. Wang, B. Deng, H. Chen, X. Wang and J. Zheng, *Environ. Sci. Technol.*, 2009, **43**, 5223–5228.

43 H. Cui, Y. Qian, Q. Li, Q. Zhang and J. Zhai, *Chem. Eng. J.*, 2012, **211**, 216–223.

44 M. Králik, *Chem. Pap.*, 2014, **68**, 1625–1638.

45 M. A. Al-Ghouti, J. Li, Y. Salamh, N. Al-Laqtah, G. Walker and M. N. Ahmad, *J. Hazard. Mater.*, 2010, **176**, 510–520.

46 M. Tabrizchi, *Talanta*, 2004, **62**, 65–70.

47 Y. M. Kim, D. Park, D. S. Lee and J. M. Park, *J. Hazard. Mater.*, 2008, **152**, 915–921.

48 K. Knox, *J. Chem. Educ.*, 1985, **62**, 863.

49 S. Alafnan, A. Awotunde, G. Glatz, S. Adjei, I. Alrumaih and A. Gowida, *J. Pet. Sci. Eng.*, 2021, **207**, 109172.

50 M. Vigdorowitsch, A. Pchelintsev, L. Tsygankova and E. Tanygina, *Appl. Sci.*, 2021, **11**, 8078.

51 X. Chen, *Information*, 2015, **6**, 14–22.

52 J. Skopp, *J. Chem. Educ.*, 2009, **86**, 1341.

53 J. Loeb, *J. Gen. Physiol.*, 1920, **2**, 673–687.

54 A. Sanjabi, S. Azizian, M. Torabi, M. A. Zolfigol and M. Yarie, *Microporous Mesoporous Mater.*, 2023, **348**, 112367.

55 M. L. Rahman, S. A. Shamrih, N. A. Azlyzan, M. S. Sarjadi, S. E. Arsad, S. M. Sarkar and S. Kumar, *Carbohydr. Polym. Technol. Appl.*, 2025, **9**, 100633.

56 M. A. Badsha, M. Khan, B. Wu, A. Kumar and I. M. Lo, *J. Hazard. Mater.*, 2021, **408**, 124463.

57 X. Yang, Y. Wan, Y. Zheng, F. He, Z. Yu, J. Huang, H. Wang, Y. S. Ok, Y. Jiang and B. Gao, *Chem. Eng. J.*, 2019, **366**, 608–621.

58 M. D. G. de Luna, E. D. Flores, M. C. B. Cenia and M.-C. Lu, *Bioresour. Technol.*, 2015, **192**, 841–844.

59 T. Anirudhan and S. Sreekumari, *J. Environ. Sci.*, 2011, **23**, 1989–1998.

60 R. Zhang, Y. Zhou, X. Gu and J. Lu, *Clean:Soil, Air, Water*, 2015, **43**, 96–103.

61 M. Monier and D. Abdel-Latif, *J. Hazard. Mater.*, 2012, **209**, 240–249.

62 X.-Y. Zhang, Q.-C. Wang, S.-Q. Zhang, X.-J. Sun and Z.-S. Zhang, *J. Hazard. Mater.*, 2009, **168**, 1575–1580.

63 Z. Wang, J. Xu, Y. Hu, H. Zhao, J. Zhou, Y. Liu, Z. Lou and X. Xu, *J. Taiwan Inst. Chem. Eng.*, 2016, **60**, 394–402.